# Localized microjetting in the collapse of surface macrocavities

K. L. Olney, P.-H. Chiu, D. J. Benson, A. Higgins, M. Serge, and V. F. Nesterenko

# Localized microjetting in the collapse of surface macrocavities

K.L. Olney[1], P.-H. Chiu[2], D.J. Benson[3], A. Higgins[4], M. Serge[4], V.F Nesterenko[1, 2]

[1]Department of Mechanical and Aerospace Engineering, University of California, San Diego, La Jolla, CA, 92093

[2]Materials Science graduate program, University of California, San Diego, La Jolla, CA, 92093

[3]Department of Structural Engineering, University of California, San Diego, La Jolla, CA, 92093

[4]Department of Mechanical Engineering, McGill University, Quebec, H3A 0C3, Canada

## Abstract

This paper focuses on the multiscale mechanism of collapse of hemispherical annular surface macrocavities in steel caused by high strain, high strain rate plastic flow of copper. Experiments and simulations revealed that a two-stage process is responsible for the observed microjetting phenomena: the formation of lateral copper microjets from the localized shear flow in copper at the interface during the filling of the cavity, and their subsequent collision at the apex of the macrocavity generating two additional horizontal microjets. The lengths of these microjets were an order of magnitude smaller than the cavity size, but linearly scaled with cavity radius. This process of microjet development is sensitive to the cavity geometry and it is unlike the previously observed jetting phenomena in cavitation, impact crater collapse, or shock-induced cavity collapse.

*Introduction* – This paper focuses on the phenomena of microjetting in the collapse of surface macrocavities. The phenomena of microjetting during cavity collapse of different initial geometries plays a crucial role in various processes such as in the collapse of *in situ* generated cavities during impact and penetration on liquid [1-3] or granular materials [4] important within the geophysical context, cavitation in a fluid near a wall [5], in generation of high velocity plasma jets [6], in explosive welding [7, 8], and in the explosively driven Thick Walled Cylinder (TWC) method [9]. The collapse of cavities is of fundamental interest due to the *in situ* self-organized flow of material with localized jetting responsible for damage due to cavitation and the generation of high amplitude localized pressures and temperatures which are important in the initiation of energetic materials and subsequent chemical reactions. Microjetting phenomena also occurs during impact of liquid droplets on solid surfaces effecting the erosion mechanism [10].

Rayleigh [11] examined the collapse of a single spherical cavity due to hydrostatic pressure and showed that, in an inviscid fluid, the velocity and pressures tend toward infinity as the size of the pore reduces to zero. Kornfeld et al. [12] were the first to observe that the collapse of cavities is unstable and suggested that this instability resulted in the generation of liquid microjets. The forced compression of cavities in liquid by a passing shock wave generates microjets [13-15].

In the cases of solid materials under shock or dynamic compressive loading, preexisting porosity/cavities in a material are preferentially collapsed. An analytical model of the symmetric collapse of spherical pores was proposed including the dependence of the mechanism of collapse on initial temperature in Carroll et al. [16, 17]. During the final stages of nonsymmetric pore collapse [18] or the shock consolidation of powders [9, 18-23], localized hotspots can be formed by the development of microjets [18]. The jet formation is influenced by the initial shape of the voids [23]. Depending on the relative amplitude of the shock to the particle strength different regimes of shock wave deformation of granular materials are observed - (a) dynamic regime with microjetting generated during pore collapse and (b) quasistatic regime of pore collapse wherein no jetting occurs [23]. This difference is important for the initiation of bonding between particles and chemical reactions under shock loading of granular materials. Shi and Brenner [24] reported that the jetting during the shock-induced collapse of nanometer-scale voids was responsible for the detonation initiation. Filling of void in porous granular materials is new mechanism of energy dissipation proposed in [25].

Mali et al. [26] showed that half spherical cavities of millimeter size scales on a free surface can generate small scale jetting caused by the shock wave interaction with the free surface of the cavity at the apex. A qualitatively similar mechanism of jetting to that reported in [26] was observed during the collapse of millimeter-sized cavity arrays in a fluid [27].

The large scale of preexisting hole (meter-sized cavity) in granite rock determines the mechanism of *in situ* crater formation due to impact by a penetrator and its evolution (permanently open crater, collapsed crater with subsequent formation of a jet moving in the reverse direction to penetration, or no crater) which influences the depth of penetration [28].

In this paper we explore the multiscale mechanisms of cavity collapse by a plastically deformed metal characterized by large strain and strain rates. Understanding of this mechanism is instrumental for optimization of material properties of filling liquid/metals and geometry of open space for maximum energy dissipation in porous granular dissipative systems, optimization of the cavity geometry for hermetic self-sealing of capsules used for storage or transportation of environmentally hazardous materials and for designing plasma generators [6] avoiding contamination of plasma by the driver material.

As we demonstrate in the present work, a qualitatively different process of microjet formation has been observed during the collapse of a hemispherical annular cavity on the interface between two metals with different strengths. Different geometry of cavity, metals used instead of water/liquid may introduce a qualitatively new feature in this process of cavity collapse, for example, due to the transition from solid to liquid-like behavior and generation of intrinsic space scales, e.g., thickness of shear localization band.

This process consists of two stages; first, a pair of lateral jets was formed due to the impact of the explosively accelerated copper (Cu) on the interface with the curved cavity during the collapse process; second, these lateral microjets converge to the apex of the cavity generating a new pair of microjets perpendicular to the impact direction. Furthermore, we show that the second pair of microjets is scaled linearly by the size of the cavity.

*Experiments* – A hemispherical macrocavity with radii of 2.79 mm was engraved into the circumference of a steel cylinder (see Fig. 1) with an outer radius of 12.5 mm. This steel cylinder was part of a larger assembly of the TWC set-up used to investigate the mechanism of plastic flow instability in various homogeneous and laminate materials [9, 29, 30]. A Cu jacket (referred to as the outer Cu driver tube in the TWC method) with a thickness of 3.38 mm was

placed on the outside of the steel cylinder. The collapse of the copper cylinder was driven by gelled nitromethane explosive (96% nitromethane, 4% PMMA) diluted 5% by mass with glass microballoons [29,30] with a thickness of 14 mm. The explosive was initiated from above to ensure a uniform detonation profile as the detonation wave passed axially along the sample.

The collapsed sample was recovered, axially cut, and images were taken of the collapsed grooves using optical microscopy (OM) and scanning electron microscopy (SEM), (see Fig. 2 and Fig. 3). Examination of the collapsed cavities revealed the following:

(1) The cavity was filled with Cu and showed only slight changes in the cavity geometry except at the apex of the cavity (Fig. 2);

(2) Localized plastic deformation occurred in the Cu adjacent to the interface with the steel on a small scale (300-500 μm in thickness) and in the immediate area near the edge of the cavity, as evident by the elongated Cu grains (see Fig. 2);

(3) The Cu showed little signs of bulk plastic strain deformation outside of the region adjacent to the interface with the steel as evident by the lack of grain distortions in the Cu (see Fig. 2);

(4) Cu microjets developed in the vicinity of the cavity apex (Fig. 2 and Fig. 3);

(5) The Cu micro-jet burrowed into the apex of the steel cavity to a depth of 250-300 μm, probably corresponding to the length of the micro-jet (Fig. 2 and Fig. 3). It is important to mention that the characteristic depth and diameter of the jet penetration is comparable to the size of localized plastic flow in Cu along its interface with the steel. Thus, the characteristic size of this localized plastic flow can be an *in situ* generated scale parameter for microjetting.

(6) Decrease of the thickness of the copper plate to 2.5 mm at the same explosive loading resulted in the similar phenomena with a similar microjet and melting of copper.

(7) The penetration depth of copper microjet into steel was similar to the penetration depth of the microjet propagating in the opposite direction into copper.

Energy dispersive X-ray spectroscopy (EDX) showed that in some of the collapsed cavities, fragments of steel were encased in the Cu adjacent to the apex of the cavity (see Fig. 3). The dramatic change of the copper microstructure observed near the apex of the cavity is characteristic of the rapid solidification of copper [31], suggesting that the copper attained

melting temperatures. Furthermore, the steel grains on the interface with the copper showed only deformation/elongation (i.e., no structural/morphological changes) confirming the absence of melting.

*Numerical modeling and Discussion* - Numerical simulations were performed in the axisymmetric geometry using the multi-material Eulerian modeling features of LS-DYNA [32], a general purpose finite element code. Finite elements with linear basis functions, one-point uniformly reduced integration, and hourglass control were used for all the calculations. Shocks were resolved using a shock viscosity with linear and quadratic terms. The solution was advanced in time using the second order accurate central difference method. This computational technology [33] was developed and validated for high strain rate, large deformation behavior of solids similar to investigated in this paper.

It was assumed that the collapse occurred under axisymmetric conditions with the initial geometry taken as the nominal dimensions of the experimental sample. The corresponding initial local geometry used in the axisymmetric simulations is presented in Fig. 1. The boundary conditions on the top and right and bottom of the domain allowed for the free flow of material out of the computational domain to avoid edge effects. The left boundary was the axis of revolution and did not allow material to move normal to the boundary, but allowed free tangential movement. The mesh resolution of the regular background mesh was chosen such that the elements had an edge length of 12.0 μm. This provided the ability to capture the *in situ* generated small space and time scale phenomena such as the localized shear flow and the microjetting. Due to the nature of the multi-material finite element formulation, the interface between the Cu and steel was assumed to be bonded and the movement of the materials within an individual element was controlled by a single velocity field. These conditions simulate a possible friction welding between Cu and steel and have been shown to be able to capture the interfacial behavior of materials during shock loading [23].

The dynamic behavior of copper, aluminum, and stainless steel used in the numerical simulations were modeled using the Johnson-Cook [34] constitutive model with a flow stress $\sigma_y$ of the form

$$\sigma_y = \left(A + B\bar{\varepsilon}_p^n\right)\left(1 + c\ln\frac{\dot{\bar{\varepsilon}}}{\dot{\varepsilon}_0}\right)\left(1 - \left(\frac{T-T_0}{T_m-T_0}\right)^m\right), \tag{1}$$

where $A$, $B$, $n$, $c$, $\dot{\varepsilon}_0$, and $m$ are material parameters and $\bar{\varepsilon}_p$ is the effective plastic strain, $\dot{\bar{\varepsilon}}$ is the effective strain rate, $T_m$ is the melting temperature, and $T_0$ is the room temperature. The Grüneisen equation of state in compression was used in conjunction with this constitutive model,

$$P = \frac{\rho_0 C^2 \mu \left[1 + \left(1 - \frac{\gamma_0}{2}\right)\mu - \frac{a}{2}\mu^2\right]}{\left[1 - (S_1 - 1)\mu - S_1\frac{\mu^2}{\mu+1} - S_3\frac{\mu^3}{(\mu+1)^2}\right]^2} + (\gamma_0 + a\mu)E, \tag{2}$$

and in tension,

$$P = \rho_0 C^2 \mu + (\gamma_0 + a\mu)E, \tag{3}$$

where $C$ is the sound speed in the material, $S_1$, $S_2$ and $S_3$ are coefficients in the shock velocity-particle velocity equation, $\gamma_0$ is the Gruneisen parameter, $a$ is the first order volume correction of $\gamma_0$, and $\mu = \frac{\rho}{\rho_0} - 1$ is a volumetric parameter. The initial yield strength, $A$, of the Ni and Al was calculated using the microhardness values of the Al and Ni foils. The other material parameters were taken from the literature [35] and are presented in Tables 1 and 2.


Table 1. Parameters for the Johnson-Cook constitutive model used in the simulations.

| Material | $P_0$ [g cm$^{-3}$] | $G$ [GPa] | $A$ [MPa] | $B$ [MPa] | $n$ | $c$ | $m$ | $T_m$ [K] |
|---|---|---|---|---|---|---|---|---|
| Al | 2.77 | 26.2 | 84.21 | 426.0 | 0.34 | 0.015 | 1.0 | 773 |
| Cu | 8.96 | 48.0 | 90.0 | 292.0 | 0.31 | 0.025 | 1.09 | 1356 |
| SS 304 | 7.90 | 71.5 | 100.0 | 1072.0 | 0.34 | 0.005 | 1.0 | 1670 |


Table 2. Parameters for the Grüneisen equation of state used in the simulations.

| Material | $C$ [m s$^{-1}$] | $S_1$ | $S_2$ | $S_3$ | $\gamma_0$ | $a$ |
|---|---|---|---|---|---|---|
| Al | 5328 | 1.338 | 0.0 | 0.0 | 2.0 | 0.48 |
| Cu | 3940 | 1.489 | 0.0 | 0.0 | 2.02 | 0.47 |
| SS 304 | 4570 | 1.48 | 0.0 | 0.0 | 1.75 | 0.50 |


The internal energy in Equations (2) and (3) is the energy per unit reference volume. It is evaluated by integrating the work performed by the stress within the element,

$$E = \frac{1}{V_0} \iint \sigma : \dot{\varepsilon} \, dt \, dV, \tag{4}$$

with the trapezoidal rule to achieve second order accuracy with unconditional stability [33]. Note that the stress includes the contributions of the plasticity through the deviatoric stress and the volumetric compression through the pressure. The temperature is evaluated by subtracting the cold compression energy $E_c(\rho)$ from the internal energy and dividing by the heat capacity,

$$T = (E - E_C)/(\rho_0 C). \tag{5}$$

The modified nitromethane explosive used in our experiments was modeled with the Jones-Wilkins-Lee (JWL) equation of state [36]

$$P = A\left(1 - \frac{\omega}{R_1 V}\right)e^{-R_1 V} + B\left(1 - \frac{\omega}{R_2 V}\right)e^{-R_2 V} + \frac{\omega E}{V}, \tag{6}$$

where $A$ = 78.69 GPa, $B$ = 1.92 GPa, $\omega$ = 0.36 , $R_1$ = 4.61, and $R_2$ = 1.06. These constants were obtained using CHEETAH 2.0 User's Manual [37]. It is assumed that the explosive in the plane of interest detonates instantaneously, since the velocity of collapse, due to relatively large thickness of copper, is significantly smaller than the detonation speed.

Images of an intermediate stage and the final stage of the cavity collapse in the simulations are presented in Fig. 4 (a) and (b) respectively. It is clear that the Cu cylinder with initial velocity of free surface 250 m/s (corresponding to a shock wave amplitude about 5 GPa) is extruded into the steel cavity which essentially maintains its initial shape as observed in experiments (see Fig. 2). This behavior can be explained by the low yield strength of Cu in comparison with the steel and also by the relatively small size of the cavity in comparison with the sizes of the steel cylinder. The thickness and location of the plastic flow of the Cu in the numerical calculations showed good qualitative agreement, with the experiments being of a similar order of magnitude (see Fig. 2), where the plastic strains can be tracked by the elongation of the copper grains. Similar to the experimental sample (where the shear localization zone in copper is shown by the interrupted lines) the thickness of the localized zone in numerical calculations was wider in the area at the edge of the cavity in comparison to the localization zone along the Cu-steel interface deeper in the cavity (Fig. 4).

It is evident from Fig. 4(a) that during the final stages of cavity collapse, a vertically oriented free surface of the central part of the Cu played a role of a "metal plate" colliding at varying angle to the steel surface which approaches a very small value as the plate nears the apex. As a result of this collision, two lateral microjets moving in the vertical plane were formed in the Cu (see Fig. 5 (a)) similar to oblique plate impact [38, 39]. But in our case, the size scale of the microjets is similar to the characteristic thickness of localized plastic flow in copper (see

Fig. 2) and not to the size of colliding plates as in previous work (see Refs. [38-42]). This *in situ* created space scale (thickness of the shear localized zone in copper) is determined by its mechanical and thermophysical properties and rate of deformation.

The remnants of these lateral microjets, identified in experiments by elongated grains in Cu, are evident in Fig. 2. For these jets to be formed ahead of the collision point, their velocities must be larger than $v_n/\sin(\gamma)$ [38, 39], where $v_n$ is the normal velocity of the free surface of the central part of the Cu. In numerical simulations at the moment shown in Fig. 4 (a), the velocity of the Cu lateral jets was ~1000 m/s, which is significantly larger than the initial particle velocity in the bulk of Cu (~250 m/s). In the investigated case of microjetting, there is no impact of two flat plates at a given angle of collision with established steady state flow in the vicinity of collision point. For this reason it is not appropriate to use quantitative comparison between our case of microjetting and collision of two flat plates [38, 39].

These lateral microjets collide at the apex prior to the impact of the planar Cu interface with the cavity apex resulting in the development of the two horizontal microjets. This process is shown in the simulations (see Fig. 5). The mechanism of horizontal microjet formation is qualitatively different than all previously observed mechanisms of microjet generation during the collapse of cavities due to shock wave loading and during the collision of metal plates described in Refs. [39-41]. The formation of two microjets caused by the collision of *in situ* generated curved crater walls in liquid and in sand was observed in [3,4].

We observed in numerical calculations that the formation of the two horizontal microjets from the two lateral microjets occurs on a very short time scale (~0.1 μs), which is two orders of magnitude smaller than the time scale of cavity collapse (~10 μs) (see Fig. 5 (a) and (c)). This difference in time scale is similar to that observed in [3] high speed jet formation after solid object impact on water.

The kinetic energy of horizontal microjets with velocity about 800 m/s (Fig. 5), found in numerical calculations, was sufficient to melt Cu, assuming that this energy was completely converted into thermal energy in a volume comparable to the volumes of the microjets. This estimate is consistent with observed localized melting in copper in places expected from numerical modeling (Fig. 3). Numerical simulations correctly predicted the similar distances of microjet penetration into steel and into copper resulting in its melting (compare Figs. 2, 3 and 6). The simulations (Fig. 6) revealed that the high strain plastic deformation resulted in the

temperature reaching the melting temperature of Cu at a distance from the interface being smaller than in experiments, the similar difference was observed for the penetration depth into steel (see Fig. 3). This disagreement is probably caused by complex behavior of high strain flow with fracture and melting of copper which was not accurately captured by the numerical calculations.

To investigate the influence of copper thickness on microjetting phenomena it was reduced from 3.38 mm to 2.5 mm maintaining the type of explosive and semispherical cavity size. A similar size of microjets was observed in experiments with these thicknesses of copper tubes suggesting that this parameter is not a scaling parameter for the microjet sizes. The microjet penetrated into the steel and melting of the copper in the opposite direction due to the trapping of the horizontal microjet similar to the previous case. Numerical simulations corresponding to this case also demonstrated similar microjetting parameters.

Additional simulations were conducted varying the size of the hemispherical annular cavities (the radii of the cavities were in the interval 0.5 and 1.5 times that were used in the experiment) to examine the relationship between the cavity size/penetration depth in the steel and the cavity size/shear localization zone thickness in Cu. Results of the simulations are presented in Fig. 7. It was found that there is a linear relationship between the penetration depth, the thickness of the localized plastic zone in the Cu, and the radius of the cavity above 0.65 of the cavity radius in experiments. This geometrical scaling revealed in numerical modeling is a strong indication that cavity collapse with other materials in conditions of loading allowing large strain plastic deformation will exhibit a cascade of microjets as presented in our paper. A similar linear scaling of the jet length with increasing bubble radius under shock-wave-induced collapse was observed in [13].

When the cavity radius (1.81 mm) was smaller than 0.65 of the experimental cavity size, microjets were not observed in the simulations. It should be mentioned that the sizes of microjets that are smaller than the resolution of the mesh (12 μm) cannot be captured in the model.

Cooper et al. [23] demonstrated that the shape of the collapsing cavity can significantly change the behavior of jetting when the cavities are on the order of $10^1$-$10^2$ μm. We performed additional simulations using two elliptical cavities with the same volume as the hemispherical cavity to examine the role of initial cavity shape on the microjetting (Fig. 8). The dimensions of the cavities were chosen such that the depth of cavity was either half or twice the depth of the

spherical cavity. In both cases, horizontal microjetting was not observed. In the former case, the collapse of the macrocavity occurred before the lateral microjets were able to converge at the apex. In the latter case, the angle of collision between the Cu and steel interface was close to 90° for the majority of the collapse process preventing formation of the lateral microjets which occurs at relatively small impact angles of collapse (for example see Fig. 4 (a)).

We also investigated collapse of the cavity with Al tube, the results are presented in Fig. 9. It is clear that this microjetting phenomena is also present for Al which has a significantly different properties than Cu.

We can conclude that he observed phenomena of microjetting is driven by its hydrodynamic nature and it is expected to occur in similar geometries with other materials when the ratio of the amplitude of shock pressure to the flow stress is of a similar order of magnitude as in our experiments (about 10, based on shock pressure 5000 MPa and copper flow stress at high strain, high strain rate 400 MPa). This scaling is similar to the proposed mechanism for the microjetting phenomena during shock densification of granular materials [19].

*Conclusions* - This paper presents the multiscale mechanism of collapse of hemispherical annular surface macrocavities in steel. This mechanism is caused by high strain, high strain rate plastic flow of copper resulting in the localized shear flow at the interface with subsequent two-stage microjetting phenomenon. This cascade of microjetting was revealed in numerical simulations. In the first stage two lateral microjets were generated between the Cu and curved cavity wall. At the final stage of collapse, these lateral jets collided at the apex of the macrocavity creating two horizontal microjets one of which penetrates into the steel. The thickness of the localized plastic zone in the Cu and sizes of microjets were scaled with the radius of the hemispherical cavity. The formation of these two horizontal microjets from the two lateral microjets occurs on time scales two orders of magnitude smaller than the time of cavity collapse. Variations of the cavity shape and size significantly influenced the microjet formation and penetration depth.

**Acknowledgment**

**References**

[1]   A. Prosperetti and H. Oguz, Annu. Rev. Fluid Mech. 25, 577 (1993).

[2]   J. Eggers, M. A. Fontelos, D. Leppinen, and J. H. Snoeijer1. Phys. Rev. Lett.,98, 094502 (2007).

[3]   S. Gekle, J. M. Gordillo, D. van der Meer, and D. Lohse, Phys. Rev. Lett., 102, 034502 (2009).

[4]   D. Lohse, R. Bergmann, R. Mikkelsen, C. Zeilstra, D. van der Meer, M. Versluis, K. van der Weele, M. van der Hoef, and H. Kuipers, Phys. Rev. Letters, 93, 198003  (2004).

[5]   C.F. Naude, A.T. Ellis, J. Basic Eng., 83, 648 (1961).

[6]   A.E. Voitenko, Doklady Akademii Nauk SSSR (in Russian), 158, 1278 (1964).

[7]   S.H. Carpenter, R.H. Wittman, Annu. Rev. Mater. Sci. 5, 177 (1975).

[8]   A.A. Deribas, Physics of Explosive Hardening and Welding, 1980, Nauka, Novosibirsk (in Russian).

[9]   V.F. Nesterenko, Dynamics of Heterogeneous Materials, Springer, New York (2001).

[10] J. E. Field, J. P. Dear, and J. E. Ogrenb, J. Appl. Phys. 65, 533  (1989).

[11] L. Rayleigh, The London, Edinburgh, and Dublin Philosophical Magazine and Journal of Science, 34, 94 (1917).

[12] M. Kornfeld, L. Suvorov, J. Appl. Phys., 15, 495 (1944).

[13] C.D. Ohl and R. Ikink, Phys. Rev. Lett., 90, 214502 (2003).

[14] J. P. Dear, J. E. Field, and A. J. Walton, Nature (London) 332, 505 (1988).

[15] N. K. Bourne and J. E. Field, J. Fluid Mech. 244, 225 (1992).

[16] M. M. Carroll and A. C. Holt, J. Appl. Phys. 43, 1626 (1972).

[17] M.M. Carroll, K.T. Kim, and V.F. Nesterenko, J. Appl. Phys. 59, 1962 (1986).

[18] A. Kapahi, H.S. Udaykumar, Shock Waves 23, 537 (2013).

[19] D.J. Benson, V.F. Nesterenko, F. Jonsdottir, M.A. Meyers, J. Mech. and Phys. Solids, 45, 1955 (1997).

[20] W. Tong, G. Ravichandran, J. Appl. Phys., 74, 2425 (1993).

[21] Z.P. Tang, W. Liu, Y. Horie, AIP Conference Proceedings, 505, 309 (2000).

[22] M.A. Meyers, D.J. Benson, E.A. Olevsky, Acta. Mater. 47, 2089 (1999).

[23] S.R. Cooper, D.J. Benson, V.F. Nesterenko, Int. J. of Plasticity 16, 525 (2000).

[24] Y. Shi, D.W. Brenner, J. Phys. Chem. C 112, 6263 (2008).

[25] Baoxing Xu, Xi Chen, Weiyi Lu, Cang Zhao, and Yu Qiao, Appl. Phys. Lett. 104, 203107 (2014).

[26] V.I. Mali, V.V. Pai, A.I. Skovpin, 1974. J. Combustion, Explosion and Shock Waves 10, 676 (1974).

[27] J.P. Dear, J.E. Field, J. Fluid Mech., 190, 409 (1988).

[28] T. H. Antoun, I.N. Lomov, L.A. Glenn, Int. J. Impact Eng., 29, 81 (2003).

[29] P.H. Chiu, K.L. Olney, A. Higgins, M. Serge, D.J. Benson, V.F. Nesterenko, Appl. Phys. Lett., 102, 241912 (2013).

[30] K.L. Olney, P.H. Chiu, A. Higgins, M. Serge, T. P. Weihs, G. M. Fritz, A. K. Stover, D.J. Benson, V.F. Nesterenko, Philos. Mag., 94, 3017 (2014).

[31] M, Suler, A. Kosec, A.C. Kneissl, M. Bizjak, K. Raic, M. Bruncko, B. Kosec, I. Anzel, Metalurgija, 14, 67 (2008).

[32] LS-DYNA Keyword User's Manual, Volume 1, Version R7.0, Livermore Software Technology Corporation (LSTC), Livermore (2013).

[33] D.J. Benson, Comput. Methods Appl. Mech. Eng., 99, 235 (1992).

[34] G.R. Johnson, W.H. Cook, Eng. Fract. Mech. 21, 31 (1985).

[35] D.J. Steinberg, Equation of state and Strength properties of selected materials, LLNL, Livermore, UCRL-MA-106439 (1996).

[36] E.L. Lee, H.C. Horning, J.W. Jury, Adiabatic expansion of high explosives detonation products, LLNL, Univ. Calif. Livermore, TID 4500-UCRL 50422 (1968).

[37] L.F. Fried, P.C. Souers, *CHEETAH 2.0* User's Manual, Lawrence Livermore National Laboratory, Livermore (1998).

[38] S.K. Godunov, A.A. Deribas, I.D. Zakharenko, V.I. Mali, J. Combustion, Explosion and Shock Waves, 7, 114 (1971).

[39] S.K. Godunov, A.A. Deribas, V.I. Mali, J. Combustion, Explosion and Shock Waves, 11, 1 (1975).

[40] M. Singh, A.K. Madan, H.R. Suneja, M.S. Bola, Int. J. Impact Eng., 11, 527 (1991).

[41] W.P. Walters, Influence of material viscosity on the theory of shaped-charge jet formation. (Report No. ARBRL-MR-02941). Army Ballistic Research Lab Aberdeen Proving Ground MD (1979).

[42] S.P. Kiselev, V.I. Mali, J. Combustion, Explosion, and Shock Waves. 48, 214 (2012).

FIG. 1. The initial local geometry of hemispherical annular cavity from the experiments used in the axisymmetric simulations. The additional investigated cavities in numerical simulations had elliptical forms with long axis in vertical (axial) and horizontal directions. Arrows show direction of shock pressure applied to copper plate due to detonation front propagating in explosive from the top to the bottom.
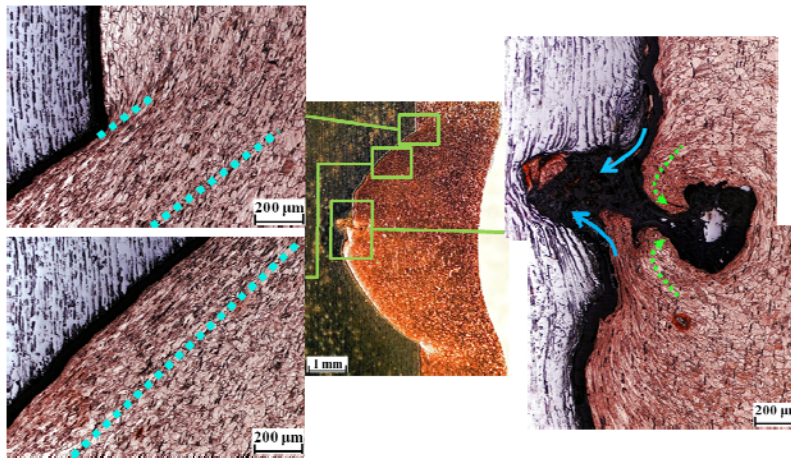


FIG. 2. Optical micrograph demonstrating the major mesoscale features of the cavity collapse. The center figure shows the collapsed cavity. The top left and bottom left insert show the localized shear flow at the vicinity of the cavity edge and along the interface of steel, respectively. The right insert demonstrates the localized shear flow in Cu (revealed by elongated grains) and directions of Cu microjets that penetrate into the steel (solid lines) and the reverse microjets that penetrate into the Cu (dashed lines) resulting from the interaction of two lateral microjets.
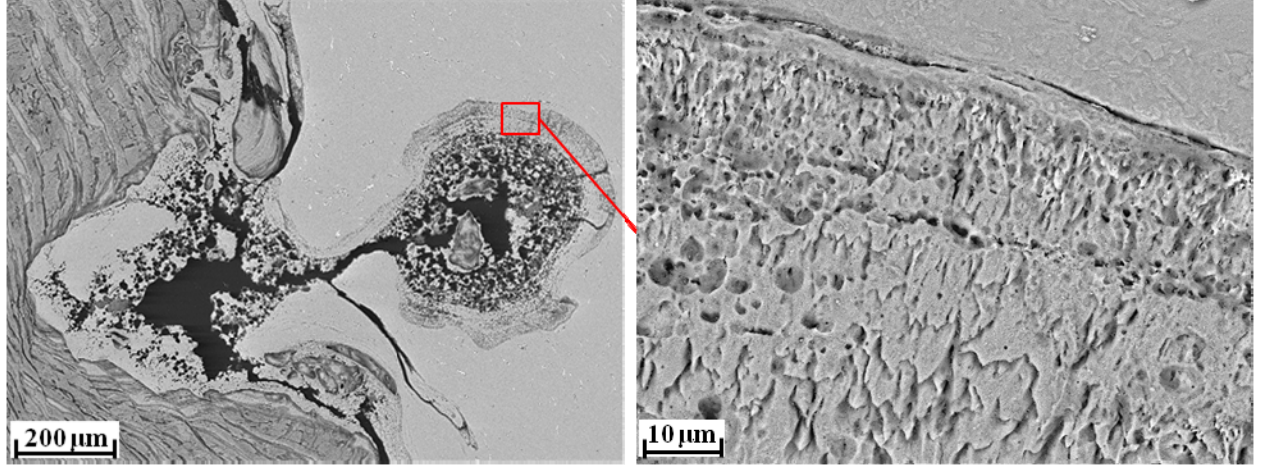
FIG. 3. A SEM micrograph demonstrating the localized melting along the interface of the microcavity in Cu created by reverse horizontal microjetting. The sharp interface between columnar microstructure is typical for rapid solidification of Cu from the fast quenching of the melt, similar to Ref. [31]. The elongated initial grains in steel demonstrate a lack of steel melting.
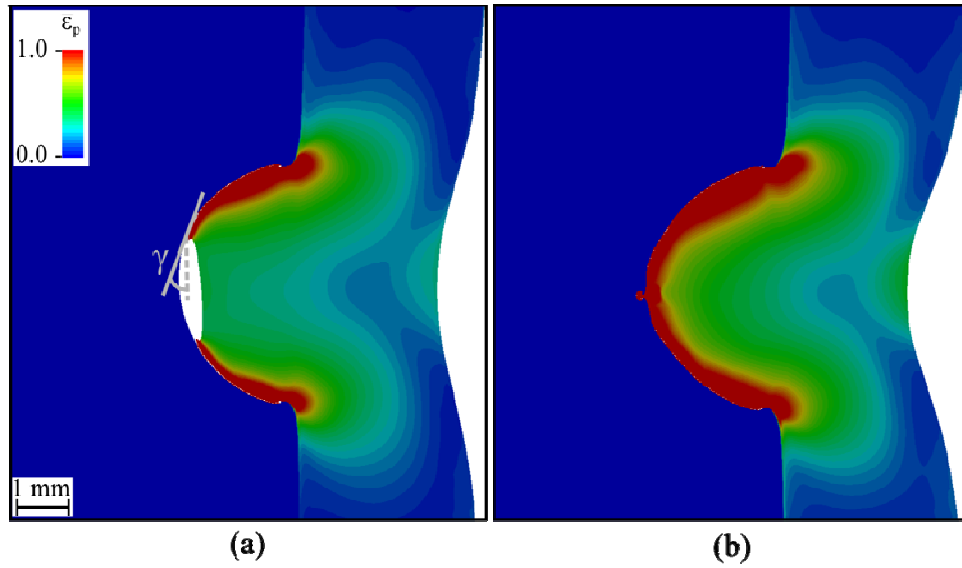


FIG. 4. The geometry, angle of collision $\gamma$, and corresponding fringe plot of the effective plastic strain at an intermediate stage (a) and after the collapse (b) of the cavity. The areas of localized plastic flow of Cu shown in red occur in the region adjacent to the steel interface. The thickness of this localized region at the end of the collapse is 800-500 $\mu$m and is two times thicker in the area near the edge of the cavity in comparison with the bottom, similar to the experimental sample (see Fig. 2, left inserts).
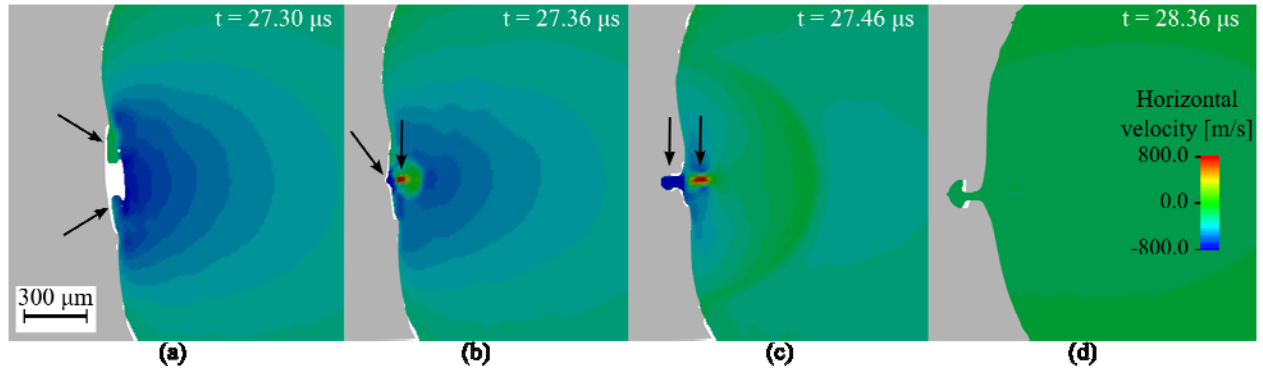
FIG. 5. The two-step mechanism of lateral and horizontal microjets formation: (a) The two lateral microjets (shown by arrows) in Cu formed on the interface with steel (gray); (b) and (c) Two instances in the development of two Cu horizontal microjects (shown by arrows) moving in opposite directions formed due to the collision of the two lateral microjets; (d) the end of the collapse process showing the final penetration depth of the microjet into the steel.
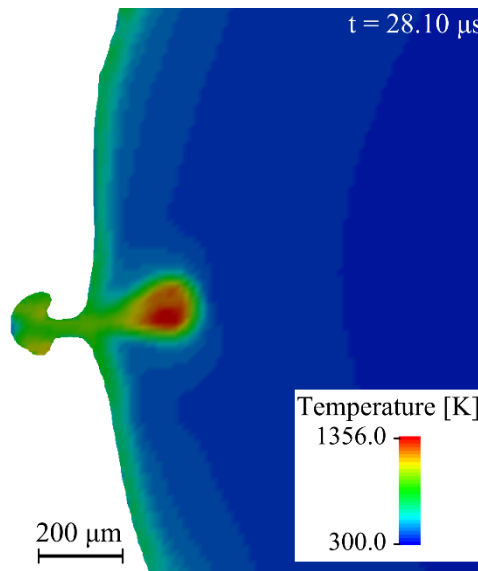


FIG. 6. Temperature in the Cu near the apex area of the cavity showing that the Cu material reaches the melting temperature. The width of microjets is comparable to the width of the localized flow in copper.
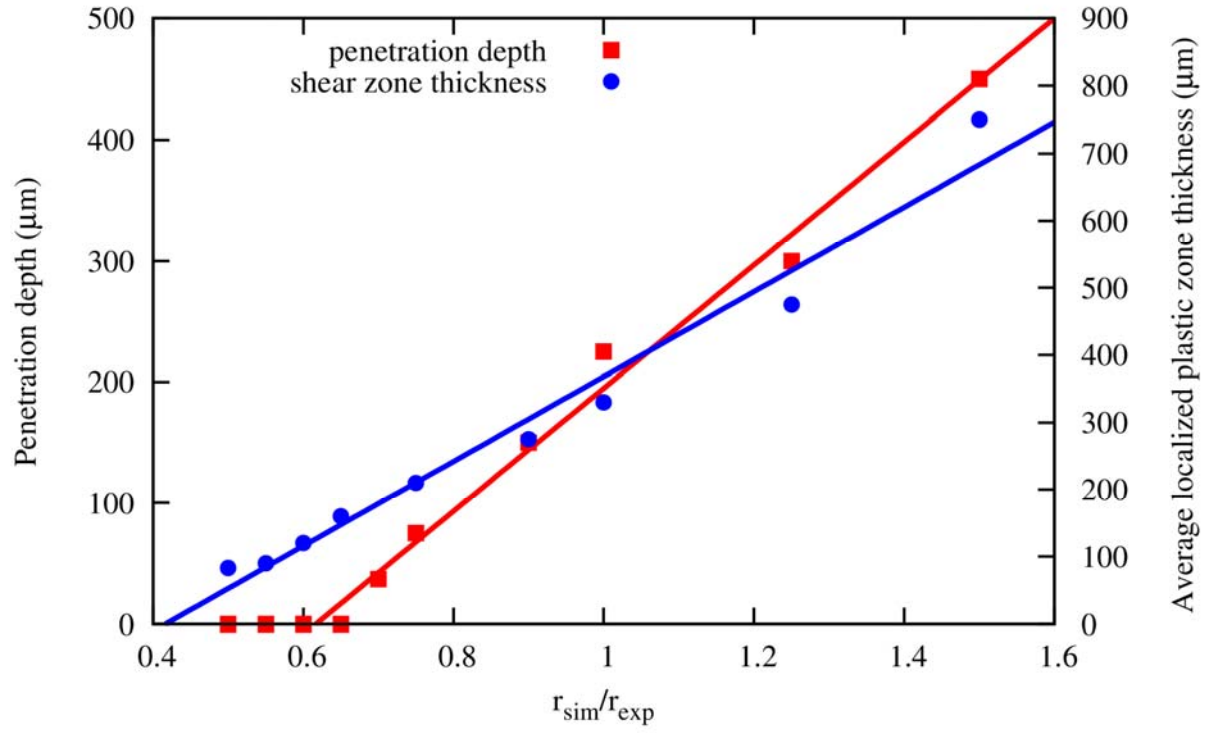
FIG. 7. Plots showing the dependence of the jet penetration depth (left axis) and average thickness of the localized shear zone (right axis), as a function of the simulated cavity radius ($r_{sim}$) normalized by the radius of the cavity in our experiment ($r_{exp}$=2.79 mm). Both the penetration depth and the shear zone thickness show a linear dependence on the radius of the cavity. Cavities with a critical radius less than 0.65 of the experimental radius do not show microjet formation.
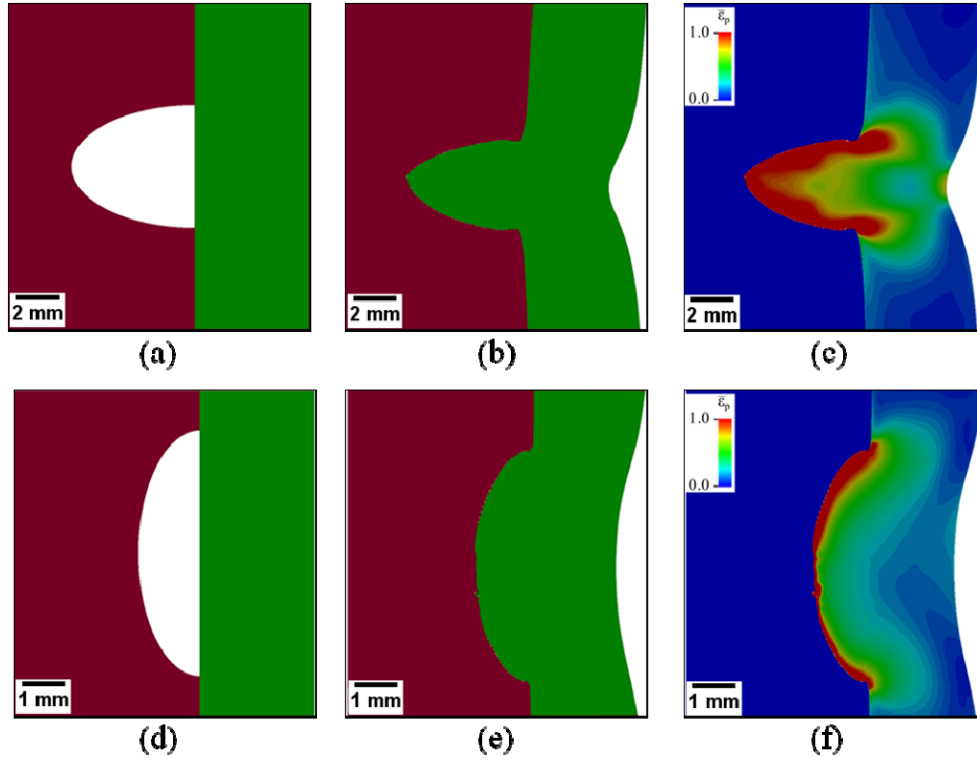
FIG. 8 Collapse of two elliptical cavities with different initial shapes in steel with the same volume as the hemispherical cavity, to examine the role of cavity shape on the microjetting. The dimensions of the cavities were chosen such that the depth of cavity was either twice ((a) to (c)) or half ((d) to (f)) the depth of the spherical cavity in experiments (Fig. 1).
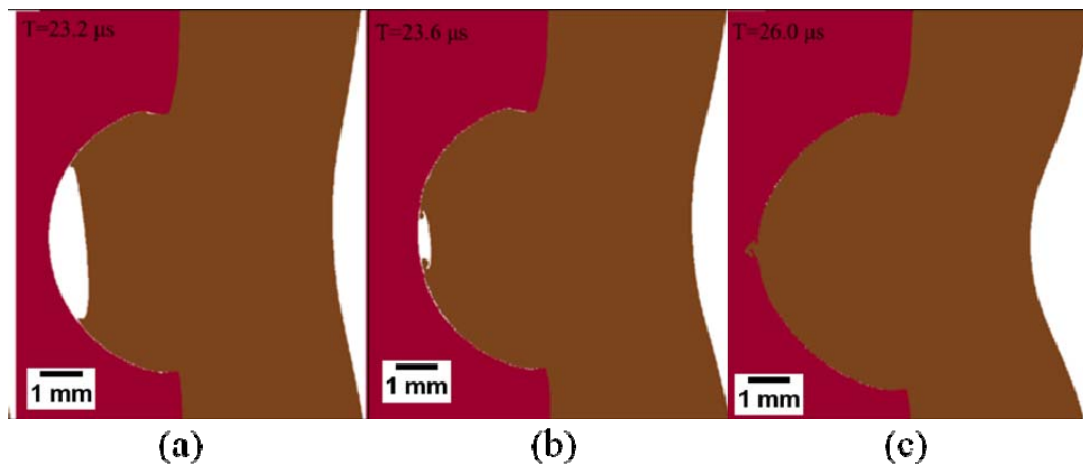


FIG. 9. Cascade of microjetting in Al at similar thickness of the Al; plate and at the same explosive loading. The red material is Steel, the brown material is Al 1100-O.